DOI 10.14622/Advances_49_2023_15

Investigation on an alternative printing plate for offset lithography

Felix Knödl[1], *Hans Martin Sauer*[1], *Jakob Feldmann*[1], *Dieter Spiehl*[1], *Andreas Blaeser*[2,3] *and Edgar Dörsam*[1]

[1] Technical University of Darmstadt, Department of Mechanical and Process Engineering, Institute of Printing Science and Technology, Magdalenenstr. 2, 64289 Darmstadt, Germany

[2] Technical University of Darmstadt, Department of Mechanical and Process Engineering, Institute for BioMedical Printing Technology, Magdalenenstr. 2, 64289 Darmstadt, Germany

[3] Technical University of Darmstadt, Center for Synthetic Biology, Schnittspahnstr. 10, 64287 Darmstadt, Germany

E-mails: knoedl@idd.tu-darmstadt.de; sauer@idd.tu-darmstadt.de; feldmann@idd.tu-darmstadt.de; spiehl@idd.tu-darmstadt.de; blaeser@idd.tu-darmstadt.de; doersam@idd.tu-darmstadt.de

Short abstract

This work investigates wetting properties of thermo and waterless printing plates commonly used in offset lithography with the goal to analyse the potential of a new printing plate making process by surface laser structuring. Measurements of the surface free energy of thermo, waterless and laser-structured aluminum samples are presented and compared. Also, the surface tension of fountain solutions and inks are measured. Laser-structured aluminum samples reached a comparable surface free energy like the waterless offset printing plate. With the help of microscopic measurement, the topography of the printing plates and the laser-structured aluminum samples were evaluated. In addition, wetting envelopes are presented which can be used to predict the wetting of a substrate with a liquid whose surface tension is known.

Keywords: wetting, laser, structure, texture, surface free energy, surface tension, wetting envelope

1. Introduction and background

Offset lithography is a commonly used printing technique that involves transferring ink from a printing plate to a rubber blanket and then onto paper. It is a highly precise and efficient process that allows for the creation of high-quality prints in large quantities. Offset lithography is widely used in the printing of books, magazines, brochures, and other commercial materials like packaging. The wetting and de-wetting properties of this printing plate play an essential role in offset lithography because it is a flat printing process and therefore the whole surface of the printing plate is in contact with the substrate. Here, non-image and image areas virtually lie in the same plane on the printing plate (Kipphan, 2000). The differentiation of ink and fountain solution is mainly controlled by chemical-physical wetting conditions. Accordingly, printing plates have different surface properties in the image and non-image areas. Particularly important is the surface free energy (SFE) of the printing plate, which can be expressed by the sum of the disperse and polar components (see Equation [4]). Equation [1] shows the regularities in contact angle determination which is the basis to further calculate the SFE;

$$\sigma_{\mathrm{sg}} = \sigma_{\mathrm{lg}} \cdot cos\,\theta + \sigma_{\mathrm{ls}} \qquad [1]$$

where σ_{lg} is the liquid surface tension, σ_{sg} is the solid surface tension, σ_{ls} is the liquid-solid interfacial tension and θ is the angle of contact for smooth surfaces defined by Young (1805). In Figure 1 the factual situation is schematically displayed.

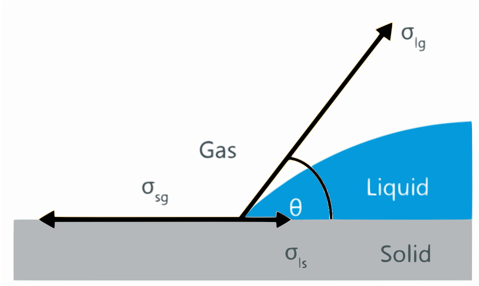

Figure 1: Wetting of a smooth solid surface with liquid surrounded by gas (Krüss, n.d.); θ: angle of contact (liquid-solid); σ_{lg}: liquid surface tension; σ_{sg}: solid surface tension; σ_{ls}: liquid-solid interfacial tension

To determine the SFE of a solid surface usually test fluids with known surface tensions are used and their angle of contact on the solid surface is measured. Typical fluids are water, ethanol, ethylene glycol, diiodomethane or glycerol. At least two fluids are needed to calculate the SFE of the solid surface to further create a wetting envelope. With the help of a wetting envelope, the wetting prediction of other fluids with known surface tension (SFT) on this solid surface can be estimated. The following Equation [2] describes the model according to Owens, Wendt, Rabel and Kaelble (OWRK) for calculating the SFE of a solid surface with disperse σ^{D} and polar σ^{P} components (Owens and Wendt, 1969; Thomsen, 2008). There are also other models but OWRK method is most suitable for this work.

$$\sigma_{\mathrm{lg}}(1+\cos\,\theta) = 2\left(\sqrt{\sigma_{\mathrm{sg}}^{\mathrm{D}}\cdot\sigma_{\mathrm{lg}}^{\mathrm{D}}}+\sqrt{\sigma_{\mathrm{sg}}^{\mathrm{P}}\cdot\sigma_{\mathrm{lg}}^{\mathrm{P}}}\right) \qquad [2]$$

For calculating the Radius $R(\theta)$ of the wetting envelope, Equation [3] and Equation [4] is used.

$$R(\theta) = \left[\left(\frac{2}{1+cos\theta}\right)\left(\frac{\sqrt{\sigma_{\mathrm{sg}}^{\mathrm{D}}\cdot cos\theta}+\sqrt{\sigma_{\mathrm{sg}}^{\mathrm{P}}\cdot sin\theta}}{cos\theta+\,sin\theta}\right)\right]^{2} \qquad [3]$$

$$\sigma_i^{\mathrm{P}} + \sigma_i^{\mathrm{D}} = \sigma_i \qquad [4]$$

Ink and fountain solution are matched to these values for the SFE, so that the fountain solution preferably adheres to the non-image areas and the ink to the image areas. The better the disperse and polar components match, the higher are the adhesion forces between printing plate (image area) and ink or printing plate (non-image area) and fountain solution (dataphysics, 2012). In general, the terms oleophilic (image area) and hydrophilic (non-image area) are used in this context, but these explicitly represent a simplified use of terms, since fountain solution does not consist exclusively of water and, in addition, the ink forms an emulsion with the fountain solution during the printing process.

Offset printing plates are approximately 0.15 mm to 0.6 mm thick anodized aluminum plates coated with a polymer. In the case of waterless offset printing plates, they have an additional silicone layer. By exposing the polymer or silicone layer with light from laser diodes, the printing and non-printing areas are created on the printing plate. In conventional printing plates, fountain solution adheres to the anodized areas and the printing ink to the remaining polymer layer. In waterless offset printing, no fountain solution is required. The ink does not adhere to the areas with a silicone layer, but likewise only to the polymer layer. For every kind of printing plate and wetting mechanism used, the printing plate, fountain solution and ink must interact perfectly (Tian, Mao and Shen, 2009).

In the early years of offset lithography, bi- or tri-metal plates were used instead of anodized and polymer coated aluminum plates (mono-metal plates). Bimetallic plates (chrome-brass) were used in web offset and trimetallic plates (chrome-copper-aluminum/iron) for sheetfed offset. Here, the metals copper and brass are considered ink-receptive, which are exposed by selectively etching the chrome layer. In small offset machines, waterproof plastic or paper printing plates were also used (Aull, 2001). Nowadays, thermal printing plates are mostly used, which are exposed with the help of infrared laser diodes. There are also special printing plates that do not require a washout process with chemicals. These are also known as *chem-free* or *process-less* printing plates, as the uncured polymer residues on the printing plates are removed by the inking and dampening rollers from the printing plate at the start of the printing process. However, these only represent a global market share of around 10 % (Nicolay, 2012).

The influence of laser-structuring on the wetting behavior of metal surfaces is currently being investigated at many research institutes and many scientific disciplines. In most cases, aluminum and steel but also other metals are processed using various laser-structuring methods (Kietzig, Hatzikiriakos and Englezos, 2009). The surface is then characterized by measuring the contact angle with water. The SFE of the manufactured samples are not carried out, but chemical analyses of the surfaces are performed and it has been recognized that the wetting properties (surface chemistry) of the metals can be altered. This can be done in common air (Dongre, et al., 2021), but can also be accelerated by using chemical treatment fluids (e.g. fluorine compounds, silicone oil). After initial laser structuring of the surface, all metals exhibit superhydrophilic wetting properties (contact angle towards less than 10°). Aging can change the wetting properties to the opposite. The surface becomes (almost) superhydrophobic (contact angle greater than 150°) (Tran and Chun, 2021).

If rough surfaces are considered, there are two possible wetting scenarios: Wenzel (1936) and Cassie-Baxter (Cassie and Baxter, 1944). Figure 2 shows these two wetting states.

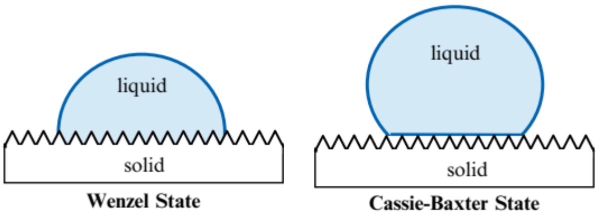

Figure 2: Illustration of the Wenzel and Cassie-Baxter state (Law and Zhao, 2016)

In the Wenzel state, the surface is completely wetted. The decisive factor here is whether the starting material is hydrophilic or hydrophobic. With hydrophilic materials, a superhydrophilic surface, i.e. spreading wetting with water, is achieved by roughening the surface. If, on the other hand, the starting material is moderately hydrophilic or hydrophobic, the wetting property increases in the direction of superhydrophobicity and water is repelled from the surface. Sometimes a metastable state in between these two states occurs, additionally vibration can transfer a hydrophobic surface to hydrophilic one (Wenzel, 1936). Equation [5] is used to calculate the contact angle θ_w in the Wenzel state:

$$\cos \theta_w = r \cdot \cos \theta \quad [5]$$

with $r = \frac{\text{actual surface area}}{\text{projected surface area}}$

In the Cassie-Baxter state, air is trapped between the rough surface and the liquid during the wetting process, and a kind of interface of air cushion is formed between the two media. This condition results in a large contact angle and the surface is superhydrophobic or even superoleophobic when wetted with water (Cassie and Baxter, 1944). Currently, a wide variety of topographic structural elements are being investigated so that the Cassie-Baxter state becomes as stable as possible and remains therefore under pressure.

As an example, the well-known *Lotus Effect* is based on the Cassie-Baxter state. Equation [6] is used to calculate the contact angle θ_{CB} in the Cassie-Baxter state:

$$\cos\theta_{\mathrm{CB}} = f \cdot \cos\theta + (f - 1) \qquad [6]$$

where f is the solid-area fraction. The aim of this work is first to determine the SFE of two common printing plates (thermo printing plate and waterless printing plate) with the help of contact angle measurement using three test fluids. Additionally, the SFT of two inks and two fountain solutions are determined and set in context to the results of the two printing plates and already published literature. Laser-structured aluminum samples with varying laser parameters are fabricated and the SFE is also be determined and examined for analogies to the printing plates. A future goal is to produce printing plates that are not based on a layer construction principle (polymer/silicone on aluminum) but can be imaged directly with a laser. For this purpose, only pure aluminum or other compatible materials are to be used.

Finally, an analogy that is already successfully used in the printing sector should be mentioned. In the flexographic printing sector, targeted surface structuring of printing plates (Kodak Flexcel NX Systems, USA and Miraclon, Belgium) has already been used for several years. This has considerably improved the uniform ink application density, dot gain and edge sharpness of the printed products, thus enhancing print quality. In Figure 3, the surface structure of one letter to be printed is shown with increasing magnification (a to d). AED stands for Advanced Edge Definition, one of the latest technologies for improving edge sharpness in flexography (James, 2021).

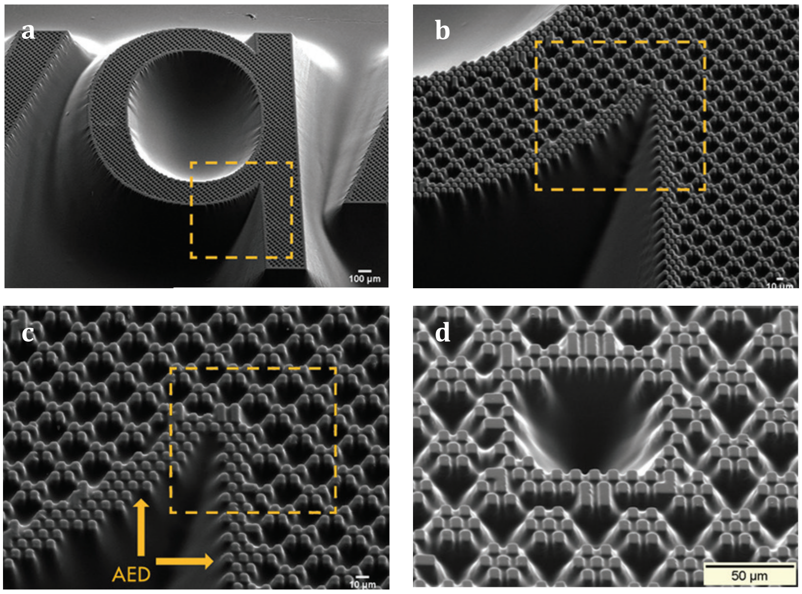

Figure 3: Detailed surface structure of a flexographic printing plate, Kodak Flexcel NX System, Miraclon's Advanced Edge Definition with surface structuring (James, 2021)

2. Materials and methods

In the following sections, the materials used and the methodology are presented. This includes the explanation of the determination of the SFT of fluids as well as the SFE of the printing plates and laser-structured aluminum samples, which were determined using contact angle measurements and a bubble pressure tensiometer. Process parameters and post-treatment of the laser-structured aluminum samples are presented and the measurement of topology of the printing plates and aluminum samples are shown.

2.1 Printing plates, inks and fountain solution

Two printing plates were investigated: a thermal printing plate *Azura TS* (Agfa, Belgium) and a waterless printing plate *Zahara Elite* (Verico Technology LLC, CT, USA). The inks tested were *Novavit 2 F100 magenta* (Flint Group, Luxembourg) and *Nevada PC cyan* (Classic Colours, Great Britain), which is used in waterless offset lithography. The fountain solutions tested were *Fluid Rotaprint* (Reiner Gräflich, Germany) with an IPA content of 10 % and *Fluid* (Roto International, Germany). Based on the odor development, it can be assumed that considerably less isopropanol is mixed in the fountain solution fluid from Roto International.

2.2 Laser structuring of aluminum samples and post-treatment

For fabrication of laser-structured aluminum samples a nanosecond fiber laser *F-9020* (KBA, Germany) was used, which has a wavelength of 1 062 nm, a spot diameter of 53 µm, a range of frequency from 20 kHz to 80 kHz, a max. laser power of 20 W, a focal length of 200 mm and a work area of 100 mm × 100 mm. Laser parameters are shown in Table 1.

Table 1: Laser parameters for fabrication of the laser-structured aluminum samples

Parameter	Values
Hatching distance	0.05; 0.10; 0.15; 0.20; 0.30 or 0.40 mm
Laser scan speed	125; 250; 500; 1 000; 1 500 or 2 000 mm/s
Laser power	20 W
Frequency	34.5 kHz
Hatching strategy	Cross-pattern with one pass

A total of 11 samples were prepared. Aluminum 3.0205 (99 % Al) with a material thickness of 0.15 mm was used for sample fabrication. Squares of 50 mm × 50 mm were cut and an area of 20 mm × 20 mm was laser-structured. After the laser structuring process, the aluminum samples were boiled in water for 10 min. Subsequently, the structured and dry surface was covered with a silicone oil *KF-96* (Shin-Etsu Chemical Co., Ltd., Japan) and heat treated in an oven at 200 °C for 10 min. Finally, the samples were cleaned in an isopropanol ultrasonic bath for 10 min. This procedure was performed according to Tran and Chun (2021). In this work, water contact angles of up to 170° were reached with this method.

2.3 Contact angle measurement and bubble pressure tensiometer

DSA 100 (Krüss, Germany) was used for contact angle measurement of test fluids on the printing plates and laser-structured aluminum samples (Krüss, n.d.; Thomsen, 2008). Test fluids were water, ethylene glycol and diiodomethane which were dispensed from the automatic dosing unit of the machine. The SFT for these fluids (Table 2) with disperse and polar fractions were taken from Ström, Fredriksson and Stenius (1987) for water and diiodomethane, and from Gebhardt (1982) for ethylene glycol. All drops had a volume of 2 µl and were applied by the sessile drop method. *Interpolation* algorithms to determine the contact angles were *tangent* (contact angle of 20° to 180°) and *circle* (contact angle of 0° to 20°).

Table 2: The SFT of three common test liquids including disperse and polar parts at 20 °C

SFT in mN/m	SFT (total)	SFT (disperse)	SFT (polar)
Water	72.80	21.80	51.00
Ethylene glycol	47.70	26.40	21.30
Diiodo-methane	50.80	50.80	0.00

The results of the contact angle measurement were then used to create the wetting envelopes according to the featured OWRK method, so that a prediction can be made about the wettability of the printing plates and laser-structured aluminum samples.

Since offset printing ink has a very high viscosity of 10 000 to 30 000 mPa·s (Leach, et al., 1988), the surface tension of the ink cannot be determined using a bubble pressure tensiometer (max. 500 mPa·s). The ink was therefore rolled thinly onto a coated cardboard, which was then directly examined with the three test liquids. The results are therefore analogous to the determination of the SFE of the two printing plates and the laser-structured aluminum samples.

The SFT of the fountain solutions were determined with a bubble tensiometer *BP 100* (Krüss, Germany). For this purpose, the capillary diameter of the capillary used was first determined in a beaker containing approximately 8 ml ultrapure water. Subsequently, the two damping solutions were measured with the capillary diameter determined. This is necessary because fountain solutions are surfactants that exhibit different surface tensions according to the bubble age. In order to also determine the disperse and polar components of the surface tension, the fountain solutions were subsequently analyzed by means of contact angle measurement on a polytetrafluoroethylene (PTFE) substrate, since this is a theoretically purely disperse material. For this purpose, the SFE of PTFE was predetermined via the three test fluids on the *DSA 100*.

All tests for contact angle measurement as well as bubble pressure were performed at a temperature of 21 °C ± 1 °C and a relative humidity of 30 % ± 5 %.

2.4 Microscopic measurements

The confocal profilometer PLu Neox from the company Sensofar was used for topographical examination of the printing plates and the laser-structured aluminum samples. The following settings were used for the printing plates: Objective DI 50X, threshold 5 % and light 10 %. For the characterization of the laser-structured aluminum samples, the best results were obtained with the following settings: SLWD 50X objective, threshold 0 % and light 4.5 %.

3. Results and discussion

In the following sections, the results on the measurements of the printing plates, the laser-structured aluminum samples, and the inks and fountain solutions are presented and then discussed. For the sake of simplicity, only a selection of the laser-structured aluminum samples is presented in detail with graphs. The selection includes the following samples:

- S1 (Scanning speed: 500 mm/s; Hatching distance: 0.20 mm)
- S2 (Scanning speed: 500 mm/s; Hatching distance: 0.15 mm)
- S3 (Scanning speed: 500 mm/s; Hatching distance: 0.10 mm)
- S4 (Scanning speed: 500 mm/s; Hatching distance: 0.05 mm)

3.1 Results of microscopic measurements of printing plates and laser-structured aluminum samples

Figure 4 shows the topographic examinations of the two printing plates. In addition, a section of a photograph of both printing plates has been added for illustration purposes. As mentioned in the introduction, offset lithography is a flat printing process in which image and non-image area lies on the same plane. However, this is technically not correct, as microscopic observation reveals that there is actually a height difference of about 2 µm to 4 µm between image and non-image areas. For the thermal printing plate (Azura TS), the image area is higher and for the waterless printing plate, the imaging area is lower compared to the non-imaging area. This is plausible because the layer structure of the printing plates differs. It can also be seen that the thermal printing plate has a much rougher surface than the waterless offset printing plate. This is also supported by the scientific work of Pavlović, Novaković and Cigula (2012) and Shen, et al. (2008), among others.

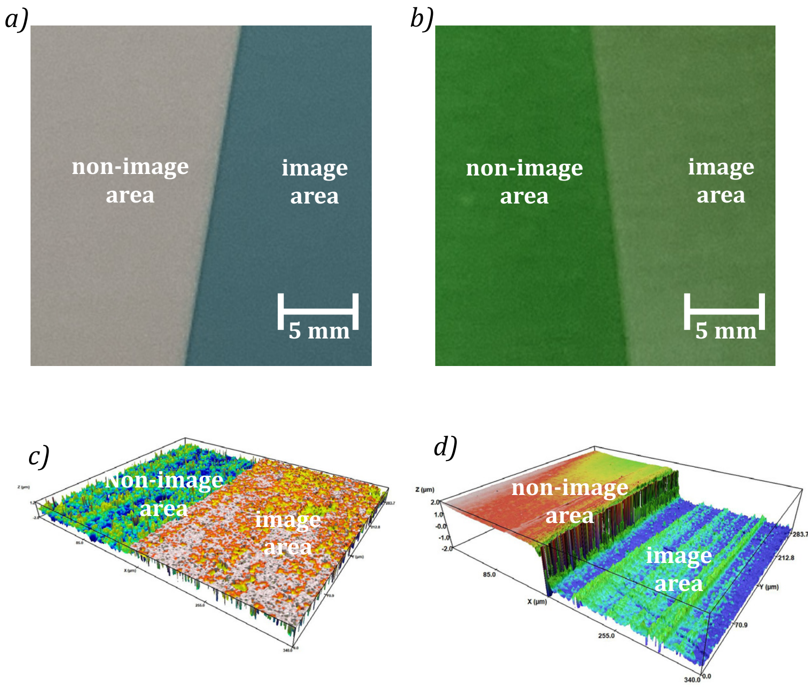

Figure 4: Image detail of thermal offset printing plate (a); image detail of waterless offset printing plate (b); microscopic topography of thermal offset printing plate (c); microscopic topography of waterless printing plate (d)

Photographs were also taken of the laser-structured aluminum samples, which can be seen in Figure 5. Up to a hatching distance of 0.20 mm, the built hatching structures are still visible to the unaided eye. From a hatching distance of 0.10 mm to 0.05 mm, they can no longer be easily identified.

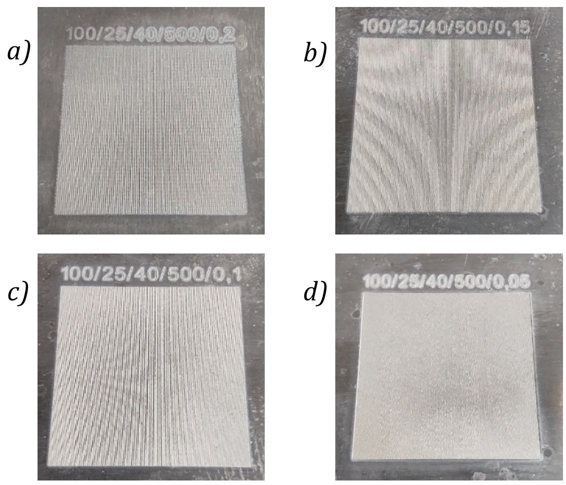

Figure 5: Image detail of selected laser-structured aluminum samples: S1 (a); S2 (b); S3 (c); S4 (d)

It should be noticed that in image detail on Figures 5a to 5c a Moiré effect appears which is not due to the laser-structuring or post-treatment rather it is of the nature from the taken pictures.

Figure 6 shows the topological analysis of the four selected laser-structured aluminum samples. The path of the laser beam is clearly visible and the hatching distance is reflected very accurately in the spacing of the valleys (blue areas). In contrast to the two printing plates, the samples have a much higher roughness. The height differences from mountains to valleys are about 50 µm to 70 µm. In sample S1, a plateau can be seen in the center, which shows the original roughness of the untreated aluminum sample.

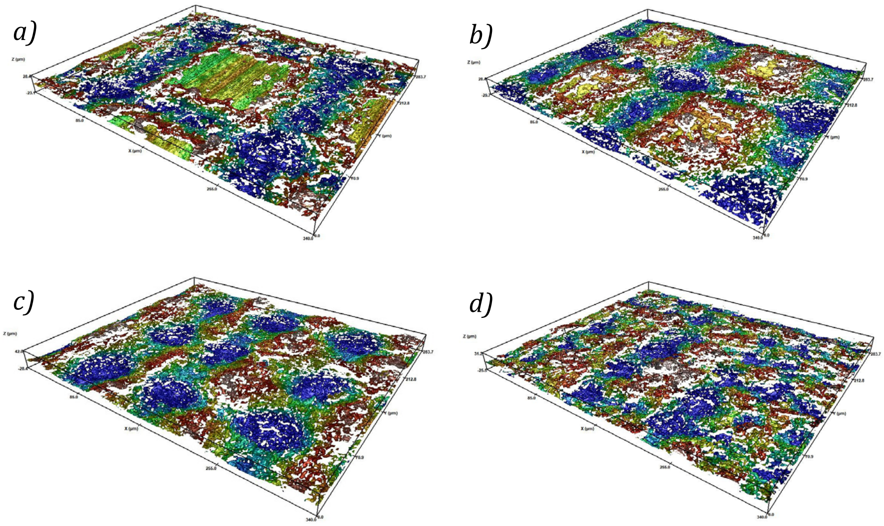

Figure 6: Topographic analysis of selected laser-structured aluminum samples: S1 (a); S2 (b); S3 (c); S4 (d)

In the following, a selection of the areal roughness parameters of the investigated surfaces of laser-structured aluminum specimens and of the imaging and non-imaging surfaces of the waterless and conventional printing plate are presented in accordance with ISO 14405-1 (Deutsches Institut für Normung, 2016). The roughness values S_a, S_z, S_k and S_q are presented in Table 3. It can be seen that the roughness parameters of the two typically used printing plates are much lower than those of the laser-structured aluminum samples. It can also be seen that the roughness values within the aluminum samples as well as the printing plates remain approximately the same.

Table 3: Surface roughness data of aluminum and printing plate samples

Sample	in µm	in µm	in µm	in µm
S1	2.04	36.75	4.67	2.91
S2	2.90	33.76	8.56	3.65
S3	3.40	38.16	10.15	4.36
S4	3.41	36.90	11.03	4.28
Zahara Elite image area	0.09	1.92	0.27	0.12
Zahara Elite non-image area	0.01	0.29	0.03	0.01
Azura TS image area	0.26	4.88	0.73	0.36
Azura TS non-image area	0.34	4.31	1.04	0.44

3.2 Contact angle measurement, SFT/SFE calculation and modelling of wetting envelopes

In this section, the contact angle measurements and the resulting SFE as well as SFT are presented. Finally, selected wetting envelopes are shown and placed in the scientific context. Figure 7 shows an example of how contact angle measurements were performed with the test fluids mentioned in the materials and methods section on the laser-structured aluminum specimens that were post-treated with silicone oil and heat. Contact angles are not explicitly listed because the later presented wetting envelopes can be used to predict the wetting with liquids for which the SFT with disperse and polar fractions is known or has been determined experimentally.

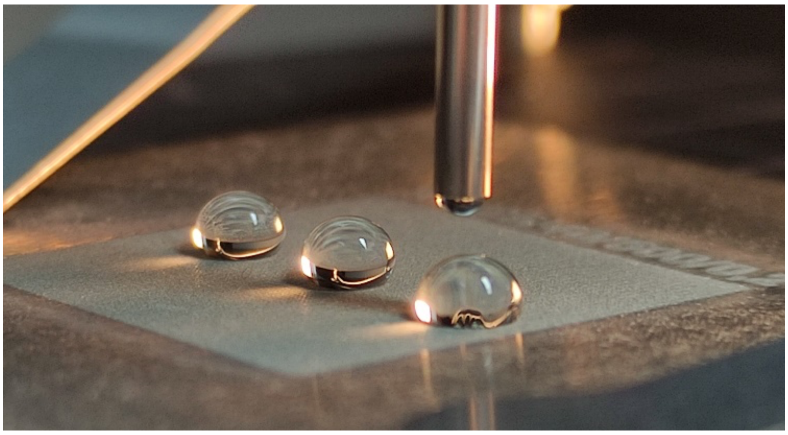

Figure 7: Contact angle measurement of laser-structured aluminum sample with ethylene glycol

The results for determining the SFE of the printing plates are listed in Table 4. In general, it can be seen that the *Azura TS* thermal printing plate has a significantly higher SFE than the *Zahara Elite* waterless printing plate. In addition, it can be seen that the Azura TS has approximately equal polar and disperse fractions. In contrast, the waterless printing plate Zahara Elite exhibits almost exclusively disperse fractions in the SFE. The results are in line with scientific work already carried out to determine the SFE of printing plates. In this context, Deshpande (2011); Cigula, et al. (2010); Tian, Mao and Shen (2009) and dataphysics (2012) can be mentioned. The results of the tests on inks and fountain solutions, which are listed in Table 4, can also be confirmed with the just mentioned scientific work. MacPhee (1998) investigated various relevant SFE and SFT of an offset printing press. The imaging area of a printing plate showed an SFE (total) of 39.4 mN/m with a disperse fraction of 36.5 mN/m and a polar fraction of 2.9 mN/m. For the non-imaging area of the printing plate, an SFE (total) of 69.4 mN/m with a polar fraction of 44.6 mN/m and a disperse fraction of 24.8 mN/m was determined. These values are comparable in magnitude to those found in this work for the Azura TS thermal printing plate. The properties of the non-imaging areas agree well. The properties of the imaging areas are further apart. This could be due to the fact that it is not clear which type of printing plate was investigated.

Table 4: SFE of thermo printing plate and waterless printing plate incl. polar and disperse parts

SFE in mN/m		SFE (total)	SFE (disperse)	SFE (polar)
Printing plate Zahara Elite	Image area	21.02 ± 1.11	21.01 ± 1.09	0.01 ± 0.01
	Non-image area	12.48 ± 1.29	11.96 ± 1.09	0.52 ± 0.21
Printing plate Azura TS	Image area	57.73 ± 1.60	36.03 ± 0.22	21.70 ± 1.38
	Non-image area	74.09 ± 0.30	33.78 ± 0.11	40.31 ± 0.19

The results for the determination of the total SFT of the fountain solution by bubble pressure tensiometer and the subsequent determination of the disperse and polar fractions by contact angle measurement on Teflon are shown in Table 5. The following values for the SFE were determined for the PTFE substrate:

- SFT (total): 17.57 ± 1.11 mN/m
- SFT (disperse): 17.02 ± 0.92 mN/m
- SFT (polar): 0.56 ± 0.20 mN/m

These were the basis for determining the polar and disperse fractions of the fountain solutions.

Table 5: SFT of inks and fountain solutions incl. polar and disperse parts

SFT in mN/m	SFT (total)	SFT (disperse)	SFT (polar)
Novavit® 2 F100 magenta	57.50 ± 0.10	50.51 ± 0.08	6.98 ± 0.01
Nevada PC cyan	51.33 ± 2.22	50.38 ± 1.82	0.94 ± 0.40
Roto Fluid	60.01 ± 1.04	36.46 ± 2.69	23.55 ± 2.88
Rotaprint R37	38.84 ± 0.64	31.51 ± 2.28	7.33 ± 2.37

Table 6 shows the results of the determined SFE of the laser-structured aluminum samples S1 to S4 as well as the results of the other aluminum samples with varying laser parameters. In particular, it can be seen that samples S2 and S3 are close to the determined SFE (overall as well as the polar and disperse fractions) of the *Zahara Elite* waterless printing plate and would therefore be suitable for further investigation. This aspect will be discussed in more detail in section 4. The two samples with 1 500 mm/s and 2 000 mm/s laser scanning speed with a hatching distance of 0.10 mm have basic tendencies towards the SFE of the *Azura TS* printing plate and should also be further investigated. The samples with laser scanning speed of 125 mm/s, 250 mm/s and 1 000 mm/s have extremely low SFE's. It may be possible that these samples could be suitable as non-imaging areas for waterless printing plates. Only further experiments and investigations can show to what extent these samples should be followed up. Finally, it must be added that no contact angle measurement and the corresponding determination of the SFE could take place for purely laser-structured aluminum specimens, since, as addressed in the introduction, without a silicone and heat treatment the specimens formed non-measurable contact angles with the test liquids (contact angles towards 0°). In particular, they showed superhydrophilic wetting behavior for water, which in turn could be an argument for using these untreated surfaces as non-imaging areas for a printing plate that works with fountain solution.

In order to achieve extreme wetting properties, the interaction of topology (microstructures) and the chemical compounds on the micro-structured surface is crucial. The surface chemistry initially determines whether the material is hydrophobic or hydrophilic, and the surface structure further enhances the effect so that superhydrophilicity or superhydrophobicity can be achieved. The extremely low SFE (< 10 mN/m) of some aluminum samples originate from strongly hydrophobic CH_3-groups observed after silicone oil/heat treatment by Tran and Chun (2021). After laser patterning and boiling water treatment, their study also found that hydrophilic pseudo-boehmite (AlOOH) had accumulated on the surface.

Table 6: SFE of laser-structured aluminum samples including polar and disperse parts

SFE in mN/m	SFE (total)	SFE (disperse)	SFE (polar)
Alu 125/0.20	2.02 ± 0.30	1.91 ± 0.08	0.11 ± 0.22
Alu 125/0.30	1.46 ± 0.16	1.37 ± 0.13	0.09 ± 0.04
Alu 125/0.40	2.45 ± 0.14	2.34 ± 0.05	0.11 ± 0.09
Alu 250/0.20	7.00 ± 3.16	5.82 ± 2.15	1.18 ± 1.01
Alu 500/0.05 (S4)	9.24 ± 1.23	7.29 ± 0.56	1.95 ± 0.66
Alu 500/0.10 (S3)	17.62 ± 3.28	13.56 ± 1.05	4.06 ± 2.23
Alu 500/0.15 (S2)	18.66 ± 3.11	15.55 ± 2.33	3.12 ± 0.77
Alu 500/0.20 (S1)	8.51 ± 2.21	7.50 ± 1.47	1.01 ± 0.74
Alu 1 000/0.10	8.50 ± 2.68	7.62 ± 1.11	0.87 ± 1.56
Alu 1 500/0.10	34.02 ± 1.04	32.65 ± 0.76	1.38 ± 0.29
Alu 2 000/0.10	50.41 ± 2.34	39.32 ± 1.25	11.09 ± 1.08

As an example for the prediction of wetting with liquids for which the SFT with the corresponding polar and disperse fractions is known, the wetting envelopes for the two printing plates (imaging as well as non-imaging areas) are shown in Figure 8. It should be noted that the three test fluids are drawn in the diagrams. The colored curves represent specific contact angles that would be formed for a corresponding SFT constellation of the liquid to be wetted. The dashed line represents the ratio of polar to disperse fractions and the solid line reflects a polar fraction of 100 %. With the help of these wetting envelopes, a substrate to be wetted can be specifically tested with various different liquids without having to perform a manual contact angle measurement. In this sense, laser-structured aluminum samples can also be theoretically tested with different fountain solutions and inks. Due to the scope, the wetting envelopes of the laser-structured aluminum samples are not shown.

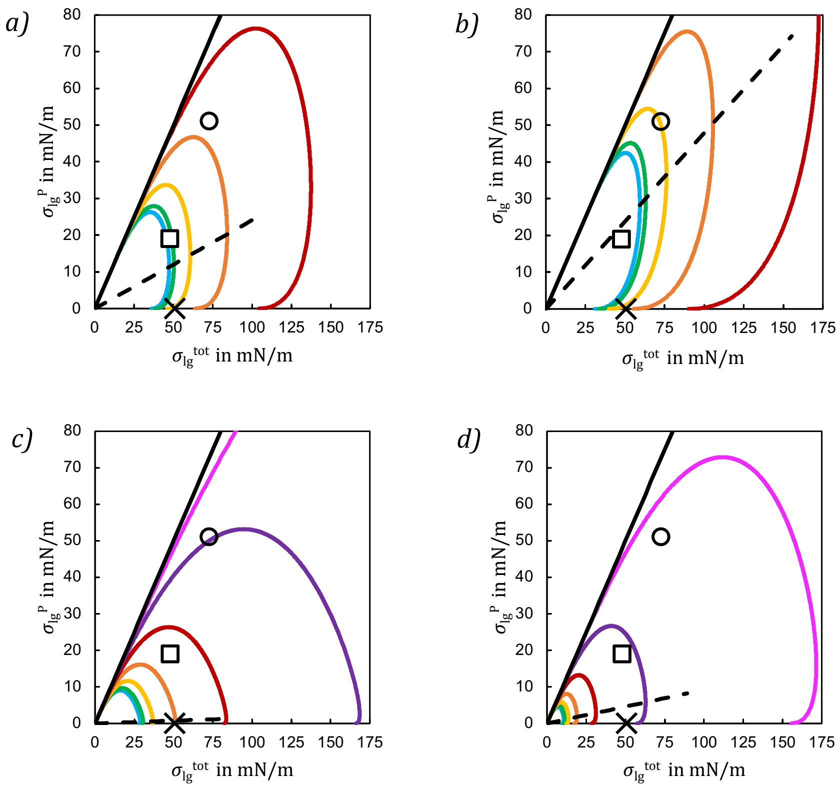

Figure 8: Wetting envelopes of thermo printing plate: (a) printing area; (b) non-printing area; and waterless printing plate: (c) printing area; (d) non-printing area (legend for contact angles of curves: light blue – 0°, green – 20°, yellow – 40°, orange – 60°, red – 80°, purple – 100°, pink – 120°; and for marks: circle – water, square – ethylene glycol, cross – diiodo-methane)

4. Conclusions

In these preliminary investigations of the laser-structured aluminum samples, it is shown that their SFE have an approximately similar value with the corresponding disperse and polar fractions of the investigated printing plates. However, the previous findings apply only to the case of static wetting. Further investigations should show whether the laser-structured aluminum surface is also compatible in the dynamic wetting case, as it occurs in offset printing presses. The influence of the surface roughness and the considerably larger height difference of the laser-structured aluminum surfaces must also be investigated in this course, since printing plates, as presented at the beginning of this chapter, have a very low surface roughness as well as height difference between imaging and non-imaging areas. Future tests should also include other metals in the investigations, such as copper, brass or bronze. Furthermore, a more suitable laser system, such as that already successfully used by Milles, et al. (2021), is to be used for surface structuring of the metal samples. With this system, hierarchical surface structures can also be created and the high resolution generally required for offset lithography can be achieved. Furthermore, the first highly dynamic wetting tests are to be started in a small-format offset press.

References

Aull, M., 2001. *Lehr- und Arbeitsbuch Druck*. 6th ed. Itzehoe: Verlag Beruf und Schule.

Cassie, A.B.D. and Baxter, S., 1944. Wettability of porous surfaces. *Transactions of the Faraday Society*, 40, pp. 546–551. https://doi.org/10.1039/TF9444000546.

Cigula, T., Pavlović, Ž., Gojo, M. and Risović, D., 2010. Wetting of offset printing plate's nonprinting areas as a function of print run. In: *Proceedings of 5th International Symposium on Graphic Engineering and Design, Grid '10*. Novi Sad, Serbia, 11–12 November 2010. Novi Sad, Serbia: University of Novi Sad, pp. 9–18.

dataphysics, 2012. *Application note 3: determination of the surface tension between a printing ink and fountain water during the offset printing process*. [pdf] Available at: <https://www.dataphysics-instruments.com/Downloads/3_Interfacial_tension_between_a_printing_ink_and_fountain_water.pdf> [Accessed April 2023].

Deshpande, S.S., 2011. Fountain solution in lithographic offset printing. *Journal of Engineering Research and Studies*, 2(2), pp. 82–88.

Deutsches Institut für Normung, 2016. *ISO 14405-1:2016-08 Geometrische Produktspezifikation (GPS) – Dimensionelle Tolerierung – Teil 1: Lineare Größenmaße*. Berlin: DIN, Beuth Verlag GmbH.

Dongre, G., Rajurkar, A., Raut, R. and Jangam, S., 2021. Preparation of super-hydrophobic textures by using nanosecond pulsed laser. *Materials Today: Proceedings*, 42(2), pp. 1145–1151. https://doi.org/10.1016/j.matpr.2020.12.497.

Gebhardt, K.F., 1982. *Grundlagen der physikalischen Chemie von Grenzflächen und Methoden zur Bestimmung grenzflächenenergetischer Größen.* Stuttgart: Fraunhofer-Institut für Grenzflächentechnik IGB.

James, A., 2021. *Enhancing print contrast.* FTA [online] Available at: <https://www.flexography.org/industry-news/enhancing-print-contrast/> [Accessed April 2023].

Kietzig, A.-M., Hatzikiriakos, S.G. and Englezos, P., 2009. Patterned superhydrophobic metallic surfaces. *Langmuir: the ACS Journal of Surfaces and Colloids*, 25(8), pp. 4821–4827. https://doi.org/10.1021/la8037582.

Kipphan, H. (ed.), 2000. *Handbuch der Printmedien: Technologien und Produktionsverfahren*. Berlin. Springer.

Krüss, n.d. *Contact angle.* [online] Available at: <https://www.kruss-scientific.com/en/know-how/glossary/contact-angle> [Accessed 12 April 2023].

Law, K.-Y. and Zhao, H., 2016. *Surface wetting: characterization, contact angle, and fundamentals*. Cham: Springer International Publishing AG.

Leach, R.H., Armstrong, C., Brown, J.F., Mackenzie, M.J., Randall, L. and Smith, H.G. eds., 1988. *The printing ink manual*. 4th ed. Wokingham, UK: Van Nostrand Reinhold.

MacPhee, J., 1998. *Fundamentals of lithographic printing: volume 1 :mechanics of printing*. Pittsburgh: GATF Press.

Milles, S., Vercillo, V., Alamri, S., Aguilar-Morales, A.I., Kunze, T., Bonaccurso, E. and Lasagni, A.F., 2021. Icephobic performance of multi-scale laser-textured aluminum surfaces for aeronautic applications. *Nanomaterials,* 11(1): 135. https://doi.org/10.3390/nano11010135.

Nicolay, K.-P., 2012. CtP und Platten: als Einheit zu betrachten. *Druckmarkt COLLECTION*, 10, pp. 3–25.

Owens, D.K. and Wendt, R.C., 1969. Estimation of the surface free energy of polymers. *Journal of Applied Polymer Science*, 13(8), pp. 1741–1747. https://doi.org/10.1002/app.1969.070130815.

Pavlović, Ž., Novaković, D. and Cigula, T., 2012. Wear analysis of the offset printing plate's non-printing areas depending on exploitation. *Tehnički Vjesnik*, 19(3), pp. 543–548.

Shen, W., Mao, Y., Murray, G. and Tian, J., 2008. Adhesion and anti-adhesion of viscous fluids on solid surfaces – a study of ink transfer mechanism in waterless offset printing. *Journal of Colloid and Interface Science*, 318, pp. 348–357. https://doi.org/10.1016/j.jcis.2007.10.016.

Ström, G., Fredriksson, M. and Stenius, P., 1987. Contact angles, work of adhesion, and interfacial tensions at a dissolving hydrocarbon surface. *Journal of Colloid and Interface Science*, 119(2), pp. 352–361. https://doi.org/10.1016/0021-9797(87)90280-3.

Thomsen, F., 2008. *Krüss technical note TN315e: practical contact angle measurement*. [pdf] Available at: <https://warwick.ac.uk/fac/cross_fac/sciencecity/programmes/internal/themes/am2/booking/dropshapeanalyser/practical_contact_angle_measurement_5.pdf> [Accessed April 2023].

Tian, J., Mao, Y. and Shen, W., 2009. Ink transfer and refusal mechanisms in waterless offset printing. *Journal of Adhesion Science and Technology*, 23(2), pp. 281–296. https://doi.org/10.1163/156856108X389442.

Tran, N.G. and Chun, D.-M., 2021. Green manufacturing of extreme wettability contrast surfaces with superhydrophilic and superhydrophobic patterns on aluminum. *Journal of Materials Processing Technology*, 297: 117245. https://doi.org/10.1016/j.jmatprotec.2021.117245.

Wenzel, R.N., 1936. Resistance of solid surfaces to wetting by water. *Industrial & Engineering Chemistry*, 28(8), pp. 988–994. https://doi.org/10.1021/ie50320a024.

Young, T., 1805. III. An essay on the cohesion of fluids. *Philosophical Transactions of the Royal Society of London*, 95, pp. 65–87. https://doi.org/10.1098/rstl.1805.0005.